

Stretchable Transparent Polyelectrolyte Elastomers for All-Solid Tunable Lenses of Excellent Stability Based on Electro–Mechano–Optical Coupling

Hao Zhong, Qiqi Xue, Jiameng Li, Yunfeng He, Yuxin Xie, and Canhui Yang*

Lenses are ubiquitously used for imaging. Compared with conventional lenses containing rigid translating components driven by mechanical motors, nonmechanical tunable lenses have been drawing attention owing to their advantages in compactness, lightweight, low power consumption, and fast response. Herein, inspired by the accommodation mechanism of the human eye, an all-solid electromechanically tunable lens driven by a dielectric elastomer actuator is presented. A soft, stretchable, transparent, and ionically conductive polyelectrolyte elastomer, poly(3-acrylamidopropyl) trimethylammonium chloride, is synthesized and used as the electrodes, one of which is plano-convex and the other planar. A mold-free procedure is elaborated to eliminate the contamination by molding and for facile fabrication. Subject to voltage, the resulting tunable lens achieves a relative change of focal length of $\approx 46.4\%$, superior to that of the human eye. The electro–mechano–optical coupling of the lens is modeled and the theoretical predictions agree well with the experimental results. Moreover, the tunable lens responds fast, operates stably in the ambient and desiccated environment, maintains performances over 1000 cycles, and exhibits a shelf-life longer than 12 weeks. The polyelectrolyte elastomer-based all-solid tunable lens promises a potential solution for lightweight, compact, and durable imaging systems.

1. Introduction

Lens apparatuses with tunable focal lengths are widely used for imaging in scenes of life. Conventional mechanical tunable lens relies on rigid-body translation to shift the lens plane using motors, which makes the lens bulky, heavy, and slow. Recently, nonmechanical tunable lenses have drawn increasing attention


owing to their advantages in compactness, cost, size, weight, response time, power consumption, and ease of fabrication.^[1–3] These unique performances are particularly beneficial when space is at a premium. Examples include portable consumer electronics (e.g., smartphones and laptops), advanced optical instruments (e.g., endoscopes,^[4] microscopes,^[5] biomimetic eyes,^[6] lab-on-chip devices,^[7] cameras for small-/micro-drones^[8] and soft robots,^[9] and virtual/augmented reality systems.^[10]

Tunable lenses generally can be categorized into three types: using liquid crystals, using a fluid medium, and using all solid components for the optical lens.^[11] Liquid crystal tunable lenses adjust the alignments of liquid crystal molecules to regulate the shape of the light wavefront in response to an applied electric field.^[12] Despite their enormous investigations, limitations have been noted such as small aperture and chromatic aberration.^[13] Fluid-based tunable lenses consist of fluids encapsulated within rigid or deformable enclosures with either constant or variable lens volume. The former changes the lens' refractive index and the latter changes the lens' shape for focal length tuning under external stimuli.^[14] For example, a droplet of conductive liquid on a solid substrate acts as a plano-convex lens, which alters the contact angle between the droplet and the substrate when a voltage is applied to trigger the electrowetting effect, resulting in the amendment of the curvature of the droplet's surface and thus the focal length.^[15] As another example, an interfacial meniscus is formed between two immiscible liquids, the curvature of which is modulated by hydraulic pressure^[16] or electrostatic force.^[17] During the past decade or so, intensive studies have focused on electro-mechanically actuating the encapsulated fluid lenses via piezoelectric actuation^[18–20] and dielectric elastomer actuators.^[21–24]

To date, the fluid-based tunable lens has developed into a relatively mature technique that commercial products are available on the market. However, the involvement of fluid in the lens brings inherent shortcomings,^[11] such as the sensitivity to gravitational sagging, mechanical vibration, thermal fluctuation, the leakage of liquid, the slow response due to inertia, and the restriction in the profile of the lens.

H. Zhong, Q. Xue, Y. He, C. Yang
Shenzhen Key Laboratory of Soft Mechanics & Smart Manufacturing
Department of Mechanics and Aerospace Engineering
Southern University of Science and Technology
Shenzhen 518055, P. R. China
E-mail: yangch@sustech.edu.cn

J. Li, Y.-X. Xie
Department of Mechanics, School of Mechanical Engineering
Tianjin University
Tianjin 300350, China

 The ORCID identification number(s) for the author(s) of this article can be found under <https://doi.org/10.1002/admt.202200947>.

DOI: 10.1002/admt.202200947

To circumvent the hindrances caused by fluid, a new class of tunable lenses composed of entirely solid components has been developed.^[11] The all-solid tunable lenses exhibit superior mechanical and thermal stability and are flexible in the design of the lens. Among the many types of all-solid tunable lenses, the ones driven by dielectric elastomer actuators additionally feature fast response, large aperture, small thickness, negligible noise, and low weight, and are becoming more and more attractive. For instance, Son and coworkers use a layer of polydimethylsiloxane membrane sandwiched between two transparent poly(3,4-ethylenedioxythiophene) electrodes to make a refractive structure.^[25] The application of voltage causes the membrane to buckle such that the curvature of the membrane is changed to vary the focal length. Pieroni and coworkers put a plano-convex polydimethylsiloxane lens in the center of an annular dielectric elastomer actuator, which squeezes the lens to bulge and reduces the focal length under voltage.^[26] More recently, soft, stretchable, and transparent ionic conductors have been employed to fabricate tunable lenses, whereby the ionic conductors function as the activating electrode and the optical lens simultaneously.^[27–28] Under actuation, the soft lens-shaped electrode accommodates the deformation of the dielectric elastomer and reduces the lens' curvature. The dual-functional ionic conductors significantly simplify the architecture and facilitate the fabrication of tunable lenses. Nevertheless, the ionic conductors implemented so far, i.e., hydrogel^[27] and ionogel,^[28] contain liquid electrolytes that can easily leak or evaporate,^[29] impeding the long-term stability of the tunable lens. Furthermore, the free ions in the electrode may diffuse through the dielectric layer to cause device failure. As such, synthesizing ionic conductors that are free of liquid electrolyte and ion leakage for all-solid stable tunable lenses is highly desired yet remains an unmet challenge.

Herein, we meet the challenge by synthesizing a polyelectrolyte elastomer, poly(3-acrylamidopropyl)trimethylammonium chloride (PAPTAC), and use it as the compliant electrode to fabricate a dielectric elastomer actuator-based tunable lens. The polyelectrolyte elastomer is soft, stretchable, transparent, and ionically conductive. We develop a molding-free technique to synthesize a plano-convex polyelectrolyte elastomer in-situ on a dielectric elastomer membrane by manipulating the wetting behavior of the precursor, which eliminates the potential contamination of the lens surface during fabrication. We show that the resulting tunable lens can change its focal length by $\approx 46.4\%$. We model the electro–mechano–optical coupling behaviors of the tunable lens by invoking the nonlinear theory of dielectric elastomer and obtain satisfactory agreements between theory and experiment. We demonstrate the accommodation of the plano-convex polyelectrolyte elastomer to the deformation of the dielectric elastomer, the fast response time upon the application of voltage (≈ 140 ms), and the multidepth object imaging of the tunable lens. Moreover, we show that the unique combination of mechanical, electrical, and optical properties of the polyelectrolyte elastomer enables the lens to operate stably in both ambient and desiccated environment, maintain performances over 1000 cycles, and exhibit a shelf-life longer than 12 weeks. It is envisioned that all-solid stable tunable lenses will pave new avenues for soft, compact, lightweight, and smart vision components for broad applications.

2. Results and Discussion

As a natural tunable lens, the human eye has long been the inspiration for artificial tunable lenses. The human eye is remarkable in its sophisticated architecture and in the richness of color and information that it can detect. As shown in **Figure 1a**, the basic anatomy of the human eye for focus-tuning consists of the crystalline lens, the ciliary muscle, and the retina.^[30] Under the relaxed vision, the ciliary muscle is slack and the focal length is distant. Under the accommodated vision, the ciliary muscle contracts to thicken the crystalline lens and the lens becomes more converging, such that the focal length is closer and the diverged light rays from a nearby object can still be projected on the retina. Mimicking the function of the human eye, the dielectric elastomer actuator-based all-solid tunable lens is made of a layer of dielectric elastomer sandwiched between two layers of polyelectrolyte elastomer, with one layer being plano-convex and the other being planar (**Figure 1b**). The polyelectrolyte elastomers are connected to the external circuit via two metal electrodes. At the interfaces between the metal electrode and the polyelectrolyte elastomer, charges of opposite polarities such as the electrons in the metal and the positive ions in the polyelectrolyte elastomer accumulate to form the electric double layers (EDLs).^[31] At voltage-off state, the focal length of the lens is close. At voltage-on state, ions of opposite polarities also accumulate on the two surfaces of the dielectric elastomer to exert Maxwell stress through the thickness, causing the dielectric elastomer to reduce thickness and expand area.^[32] The plano-convex polyelectrolyte elastomer lens is soft to accommodate the deformation, resulting in the reduction of its curvature and the increase of its focal length.

Hereafter, the polyelectrolyte elastomer will be abbreviated as PEE unless otherwise specified. The PEE is composed of an elastomeric polymer network with fixed positive ions and mobile negative ions or the opposite. We select the polycation strategy by polymerizing the (3-acrylamidopropyl)trimethylammonium chloride (APTAC). The resulting poly(3-acrylamidopropyl)trimethylammonium chloride (PAPTAC) has the quaternary ammonium ions anchored to the polymer chains and the chloride ions mobile within the polymer network (**Figure 1c**). Put in contact with a dielectric elastomer, the concentration gradient drives the ions to diffuse from the PEE into the dielectric elastomer. However, such long-range diffusion of ions is arrested since the elasticity of PEE holds the positive ions within the network meanwhile the migration of the negative ions is prohibited due to the electrostatic interactions. Because PAPTAC is arranged along the optical path, its transparency is of great importance for the overall transparency of the tunable lens. We measure the transmittance of a piece of $500\ \mu\text{m}$ PAPTAC over the range from 400 to 800 nm and obtain an average transmittance of $\approx 93\%$ (**Figure 1d**). Mechanically, uniaxial tensile stress–strain curves indicate that PAPTAC has an elastic modulus of 40.5 ± 5.8 kPa and fracture strain $>600\%$ (**Figure 1e**), which favors the PAPTAC to adapt to the deformation of the dielectric elastomer with minimal constraint. Electrically, PAPTAC needs to conduct electricity for actuation and its conductivity is measured to be on the order of $10^{-2}\ \text{S m}^{-1}$ within the temperature range from 10 to 65 °C (**Figure 1e**). The escalation of the conductivity is attributed to the increase of ion mobility at elevated temperature.

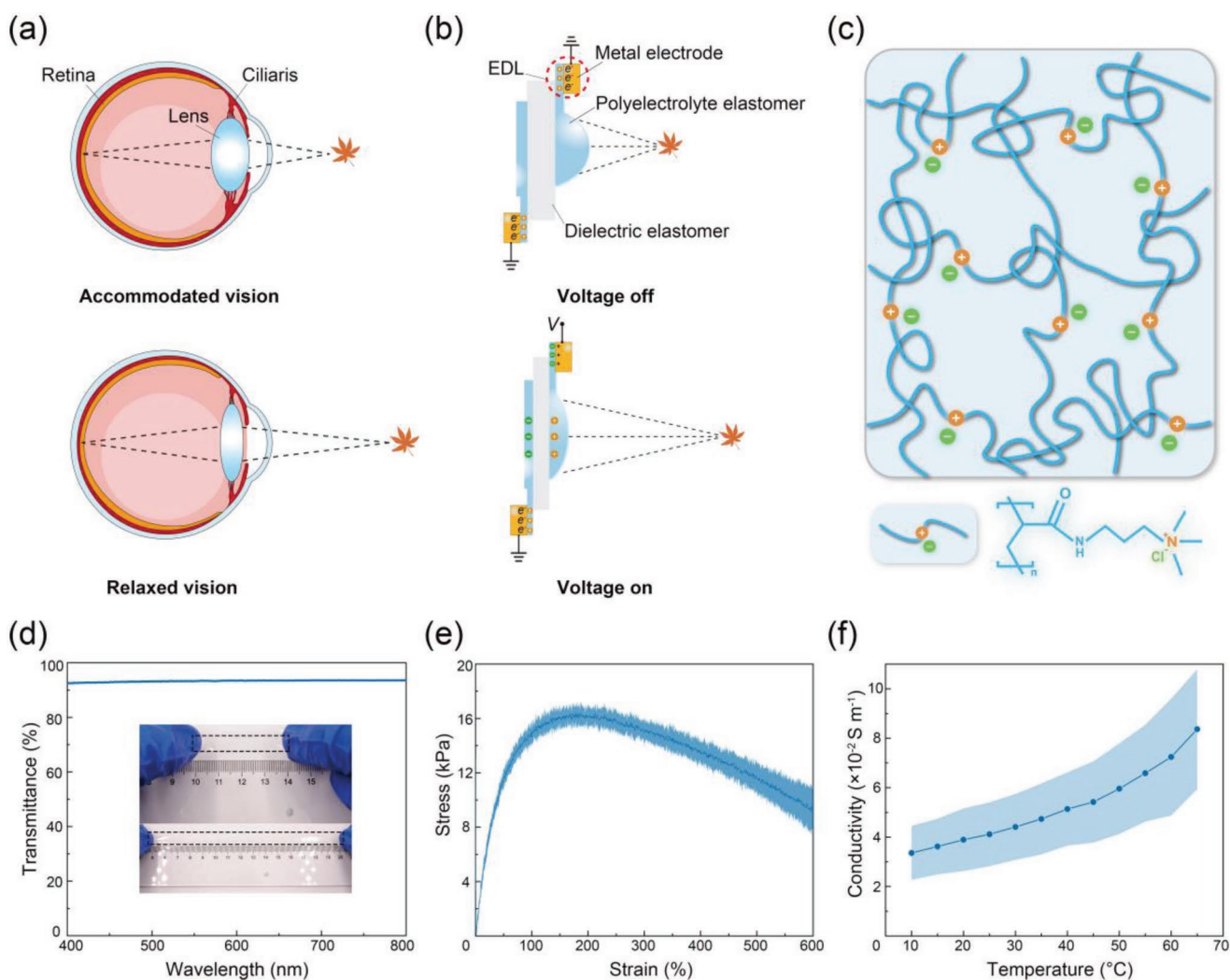


Figure 1. Mechanism of tunable lens and performances of polyelectrolyte elastomer. a) The basic structure and focus-tuning mechanism of the human eye. The ciliary muscle contracts to deform the crystalline lens upon accommodated vision, which shortens the focal length, and relaxes to flatten the crystalline lens under relaxed vision, which lengthens the focal length. b) The basic structure and principle of the polyelectrolyte elastomer-based tunable lens driven by a dielectric elastomer actuator. The radius of curvature of the lens is small and the focal length is short in the voltage-off state, and the lens is stretched to increase the radius of curvature and the focal length becomes farther in the voltage-on state. c) Schematic of the network of PAPTAC and the molecular structure of APTAC. d) The transmittance of 500- μm -thick PAPTAC. The insets show a highly transparent PAPTAC strip in original and stretched ($\lambda \approx 4$) states. e) Uniaxial tensile stress–strain curve of PAPTAC. f) The conductivity of PAPTAC varies with temperature. The shaded regions in (e) and (f) indicate the bandwidths of the error bars. The sample size is $n = 3$ for (d–f).

We then use the PEE with ideal mechanical, electrical, and optical properties to fabricate a tunable lens. The crucial part is the synthesis of the solid lens.^[28,33] which is often intricate, time-consuming, and susceptible to defects and/or contaminations. In this regard, we develop a mold-free technique to directly synthesize a plano-convex polyelectrolyte elastomer in-situ on a dielectric elastomer membrane. As illustrated in **Figure 2a**, a layer of an acrylate adhesive (VHB 4910, 3M) is prestretched biaxially to $\lambda_{\text{pre}} \approx 3.3$ (Figure S1, Supporting Information) and fastened to a circular polymethyl methacrylate (PMMA) frame. After being cutoff, VHB is masked by a piece of annular polyester and subjected to plasma etching. Subsequently, the mask is removed and a certain volume of PEE precursor is dripped on the plasma-etched region. After that, the sample is placed

inside a humid chamber of nitrogen atmosphere and exposed to ultraviolet illumination for curing. Finally, the sample is taken out and additional planar PEEs and metal electrodes are installed to construct the all-solid tunable lens. The key to the molding-free fabrication process lies in the spontaneous and stable wetting of the PEE precursor within the plasma-etched region. During the plasma-etching process, the hydrophobic acrylate ester moieties on the surface of VHB are oxidized into hydrophilic moieties (e.g., $-\text{OH}$) (Figure 2b). As a result, the surface energy of the plasma-etched region (in purple) becomes higher than that of the unetched region. In addition, the surface energy of the PEE precursor is lower than the former but higher than the latter (Figure S2, Supporting Information), such that the PEE precursor of appropriate volume will wet and stay within the plasma-etched region.^[34] Furthermore, the

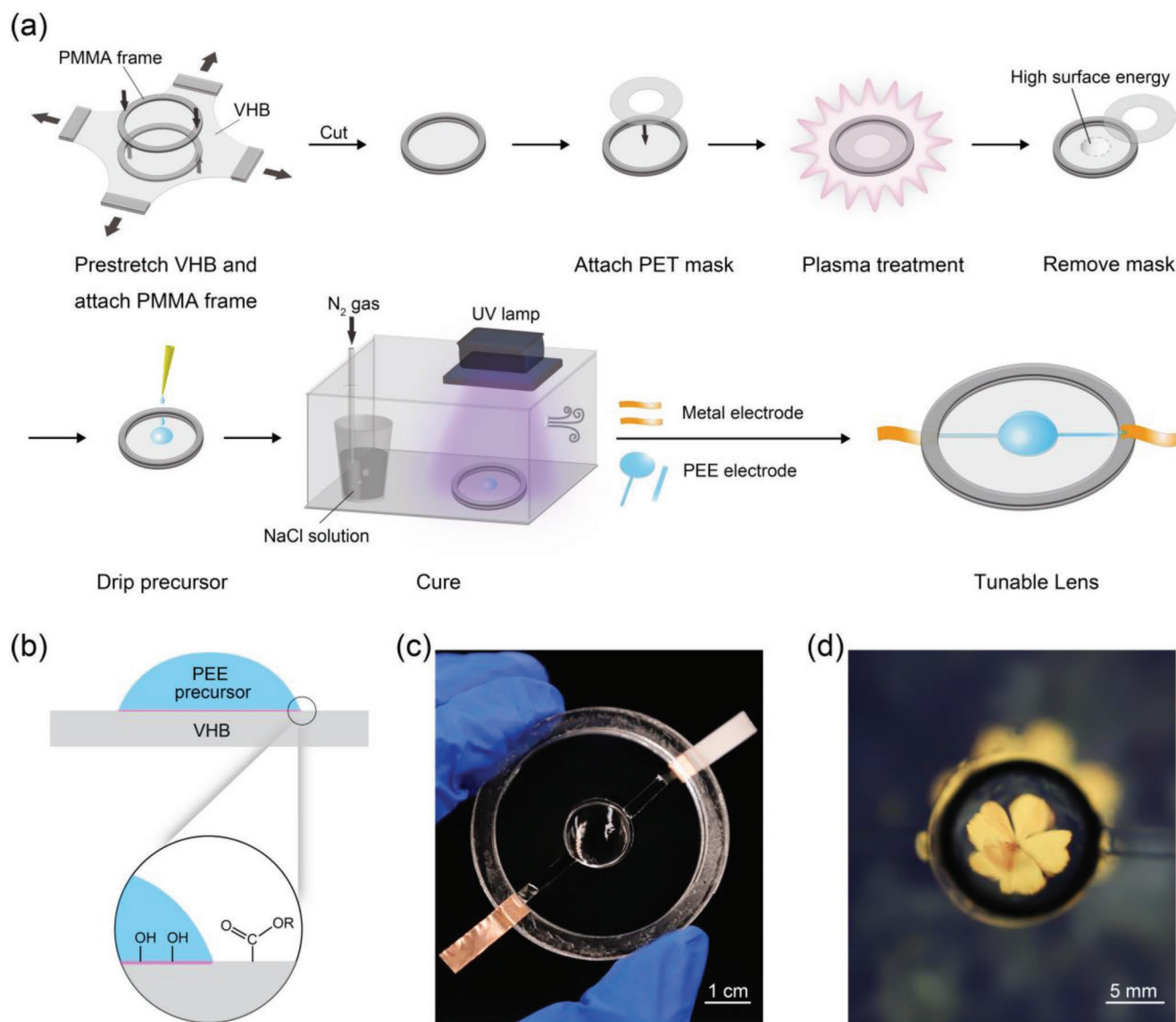


Figure 2. Mold-free fabrication of tunable lens. a) Schematic of the fabrication process. b) Schematic illustrating the wetting of the precursor of PAPTAC (in blue) on the surface of VHB. Plasma converts the hydrophobic acrylate ester moieties into hydrophilic moieties (e.g., $-\text{OH}$), resulting in the increase of surface energy (in purple). c) The overall appearance of the PEE-based tunable lens. d) A photo of a flower on a laptop screen taken through the lens.

droplet of PEE precursor retains its profile with a high degree of fidelity after curing (Figure S3, Supporting Information).^[35] Figure 2c exemplifies the overall appearance of an as-prepared PEE-based tunable lens with a basal diameter of 15 mm and a volume of 450 μL . Figure 2d shows a photo of a yellow flower on a laptop screen seen through the lens.

Next, we quantify the focus-tuning performances of the tunable lens. As schematized in Figure 3a, we fasten the lens vertically and place two beams of parallel light on the side of the base of the lens and a screen ahead of the lens' curved surface. The parallel light forms a light spot on the screen after passing through the lens. By moving the screen relative to the lens, the size of the spot changes. Focal length is determined as the distance between the screen and the base center of the lens when the spot is the smallest. At voltage-off state, the focal length is

measured as 20.7 ± 1.5 mm. For a plano-convex lens in air, the focal length can be estimated as:

$$\frac{1}{f} = \frac{(n-1)}{R} \quad (1)$$

where f is focal length, n is the refractive index of PEE, and R is the radius of curvature. Assume that the plano-convex lens is a spherical cap, then the radius of curvature relates to the geometry as:

$$R = \frac{D^2 + 4H^2}{8H} \quad (2)$$

where H and D denote the basal diameter and center point height of the lens, respectively, and are correlated through

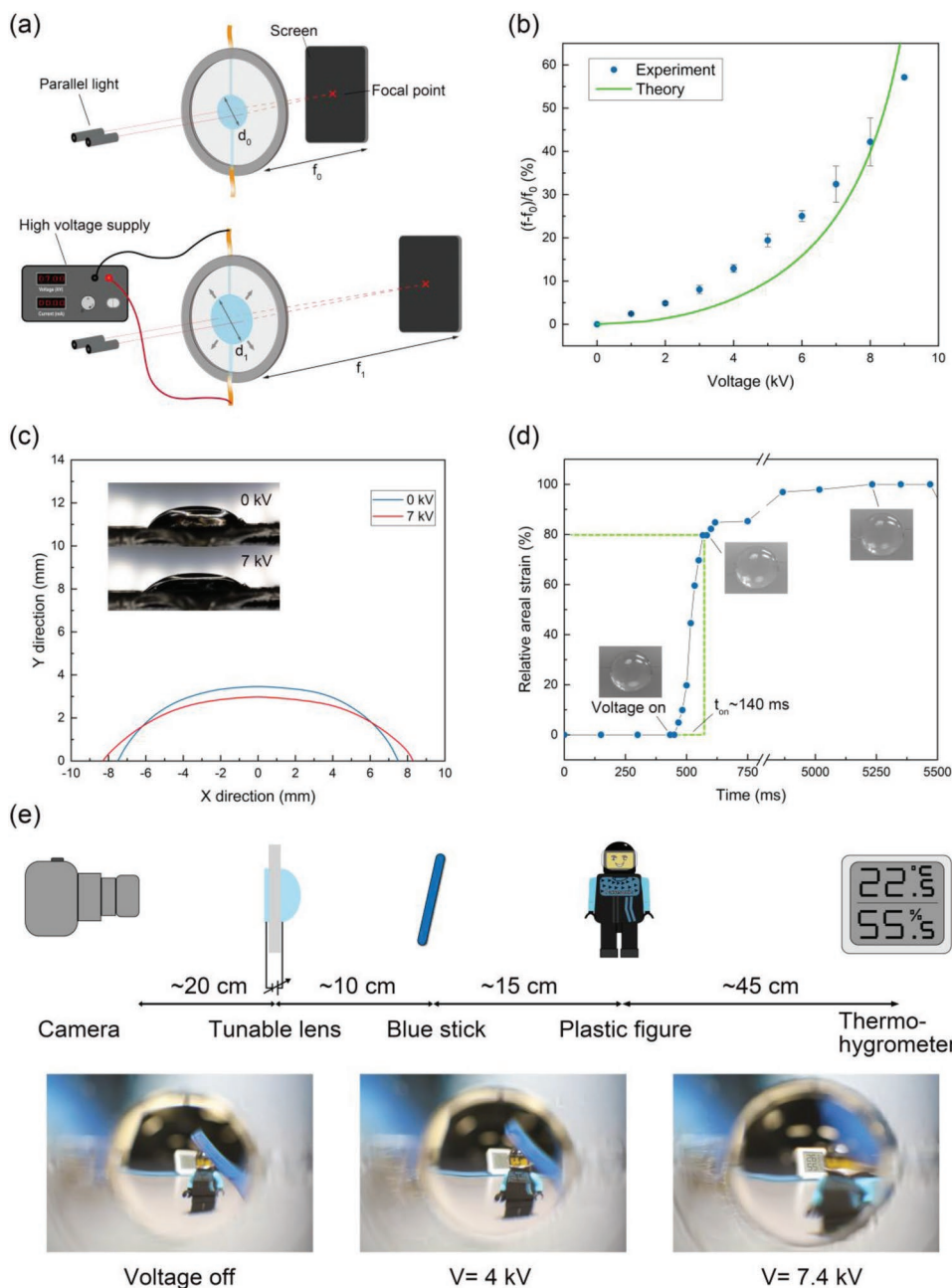


Figure 3. Performances of the tunable lens. a) Schematic of the measurement setup for the focal length of the tunable lens. b) The relative change of focal length $(f - f_0)/f_0$ varies with applied voltage. The blue dots represent experimental data, and the green curve is theoretical prediction. c) Cross-sectional profile of the tunable lens at voltage-off ($V = 0$) and voltage-on ($V = 7$ kV) states. The insets are the corresponding images. d) Relative areal strain of the tunable lens varies with time as the voltage is switched from 0 to 7 kV, giving a response time of ≈ 140 ms to reach 80% deformation. The insets are the morphologies at 0%, 80%, and 100% relative areal strain, respectively. e) Schematic and images illustrating the change of the focal length of the tunable lens subjected to voltages as indicated. The sample size is $n = 3$ for (b) and (d).

the volume as $V = \pi H(3D^2 + 4H^2)/24$. For $V = 450 \mu\text{L}$ and $D = 15$ mm, we estimate $f \approx 17.5$ mm. The discrepancy is mainly due to the deviation of the shape of the lens from a spherical cap due to gravity, and will be mitigated for lenses of small volumes where surface tension prevails. At voltage-on state, both the areal strain of the dielectric elastomer actuator (Figure S4, Supporting Information) and the focal length of the lens increase with the magnitude of voltage. The new focal length is meas-

ured by adjusting the position of the screen. A focal length of 30.3 ± 2.5 mm is achieved at 9 kV, corresponding to a relative change of focal length of $\approx 46.4\%$, which exceeds that of the human eye, $\approx 30\%$.^[24] Figure 3b plots the relative change of focal length as a function of voltage.

During the actuation, the dielectric elastomer between PEE electrodes is subjected to both mechanical stress due to pre-stretch and Maxwell stress due to electrostatic attraction. The

nonlinear deformation in the dielectric elastomer induces the plano-convex lens to deform and change focal length. Such electro-mechano-optical coupling behaviors of the tunable lens can be analyzed by invoking the theory of dielectric elastomer and geometrical optics (Figure S5, Supporting Information). Briefly, both the dielectric elastomer and PEE are considered to be incompressible and their constitutive relations are described by the Gent model:

$$W_s = -\frac{\xi J_{\text{lim}}}{2} \ln\left(1 - \frac{I_1 - 3}{J_{\text{lim}}}\right) \quad (3)$$

where W_s , ξ , and J_{lim} denote the strain energy density, shear modulus, and extension limit, respectively, and $I_1 = \lambda_1^2 + \lambda_2^2 + \lambda_3^2$ is the first invariant of the right Cauchy–Green deformation tensor, with λ_1 , λ_2 , and λ_3 being the principle stretches. In addition to strain energy, the dielectric elastomer covered with PEE electrodes also stores electrical energy,

$$W_e = \varepsilon(\phi\lambda_1\lambda_2)^2 / 2H^2 \quad (4)$$

where W_e , ε , ϕ , and H denote the electrical energy density, the permittivity, the applied voltage, and the initial thickness of the dielectric elastomer membrane, respectively. Upon actuation, the center region covered with PEE electrodes (active region) deforms homogeneously, while the peripheral annular region (passive region) deforms inhomogeneously. At the junction, force balance dictates that

$$S_r^a H + S_{\text{PEE}} H_{\text{PEE}} = S_r^p H \quad (5)$$

where S_r^a and S_r^p denote the nominal radial stress of the dielectric elastomer in the active and passive zone, and S_{PEE} and H_{PEE} denote the nominal radial stress and the equivalent initial thickness of PEE. Solving the force balance equation yields the radius of curvature of the lens in current state, which then can be used to calculate the focal length. It can be seen that theoretical prediction (green curve in Figure 3b) fits with experimental results satisfactorily.

We verify the accommodation of the PEE to the deformation of VHB by measuring the geometric morphologies of the lens without/with voltage. Indeed, the diameter of the base of the lens increases from 15 to 16.6 mm at 7 kV (Figure 3c). Such accommodation is attributed to the strong adhesion between PEE and the plasma-etched VHB, 51.2 J m⁻² (Figure S6, Supporting Information). Unlike the mechanical zooming via rigid-body motions and the digital zooming via human–machine interactions, the electrically tunable lens is fast that, when the voltage is switched from 0 to 7 kV, the area of the lens expands in hundreds of milliseconds. Define the time required for the lens to change from 0% to 80% of the maximum relative areal strain as the response time and $t_{\text{on}} \approx 140$ ms is obtained (Figure 3d). The response time is limited by the viscoelastic nature of VHB, which can be replaced by less viscous dielectrics such as silicone elastomers.^[21]

We demonstrate the multidepth object imaging performances of the tunable lens. As shown in Figure 3e, we mount different objects, including a blue stick, a plastic figure, and a thermo-

hygrometer, at different distances in front of the lens, and a digital camera behind the lens. At voltage-off state, the image of the blue stick is the sharpest, indicative of the focal plane. As the voltage increases, the images of the plastic figure and the thermo-hygrometer sequentially become sharp, with negligible chromatic and astigmatism aberrations, at 4 and 7.4 kV, while other out-of-focus objects are blurred. The blurring of out-of-focus objects in each frame signifies a small depth of field, indicative of a relatively large numerical aperture. The numerical apertures are estimated to be 1.38 to 1.83 over the entire imaging range. Higher numerical apertures can be achieved by reducing the basal diameter or increasing the radius of curvature of the lens. Further increase of voltage leads to the out-of-focus of all objects. As the voltage decreases, the three objects come into focus in reverse sequence (Movie S1, Supporting Information).

The usage of PEE for the all-solid electromechanically tunable lens has the advantages of ambient and long-term stability, compared with those involving liquid electrolytes in the electrode materials. For example, a piece of PEE maintains weight, while a piece of typical ionic hydrogel (polyacrylamide hydrogel containing 2 mol L⁻¹ sodium chloride) dries out in the open air (Figure S7, Supporting Information). We prepare two tunable lenses with PEE and the ionic hydrogel as the electrodes. Immediately after the preparation, both tunable lenses exhibit decent areal strain under 7 kV (Figure 4a). Then, we store the two lenses in a desiccated environment (≈ 12 RH%) for 24 h. The lens with PEE remains transparent while the lens with ionic hydrogel dries out and becomes opaque. The former can still be activated, albeit the areal strain drops from 18.6% to 10.6% due to the stiffening of PEE, and the latter cannot be activated at all. Afterward, we store the two lenses in the ambient environment for 24 h for recovery. The lens with PEE regains performances while the lens with ionic hydrogel remains scrapped.

To further demonstrate the long-term stability of the PEE-based tunable lens, we apply a cyclic voltage of maximum voltage of 6 kV and measure the areal strain as a function of the number of cycle (Figure 4b). Since both VHB and PEE are viscoelastic, we wait for about 5 s upon switching on and switching off to allow sufficient deformation and relaxation during each cycle. The lens remains stable for 125 cycles. We also apply a sinusoidal voltage of peak 5.7 kV and a frequency of 1 Hz in the open air and the lens maintains functions without noticeable degradation after 1000 cycles (Movie S2, Supporting Information). In addition, we examine the shelf-life of the PEE-based tunable lens by tracking the areal strains of a set of samples over time. The samples maintain functions for more than 12 weeks (Figure 4c).

It should be noted that the initial profile of the plano-convex lens predominates the performances of the tunable lens. Recall that during the molding-free fabrication, the initial profile of the plano-convex lens is almost identical with that of the precursor. Because the profile of the precursor can be tailored simply by mediating the size of plasma-etching zone and the volume of the precursor (Figure S8, Supporting Information),^[35] the molding-free procedure thus provides a facile yet effective method to regulate the focal length of the tunable lens. Also worth mentioning is that the EDLs can withstand a voltage on the order of 1 V while the working voltage of the lens

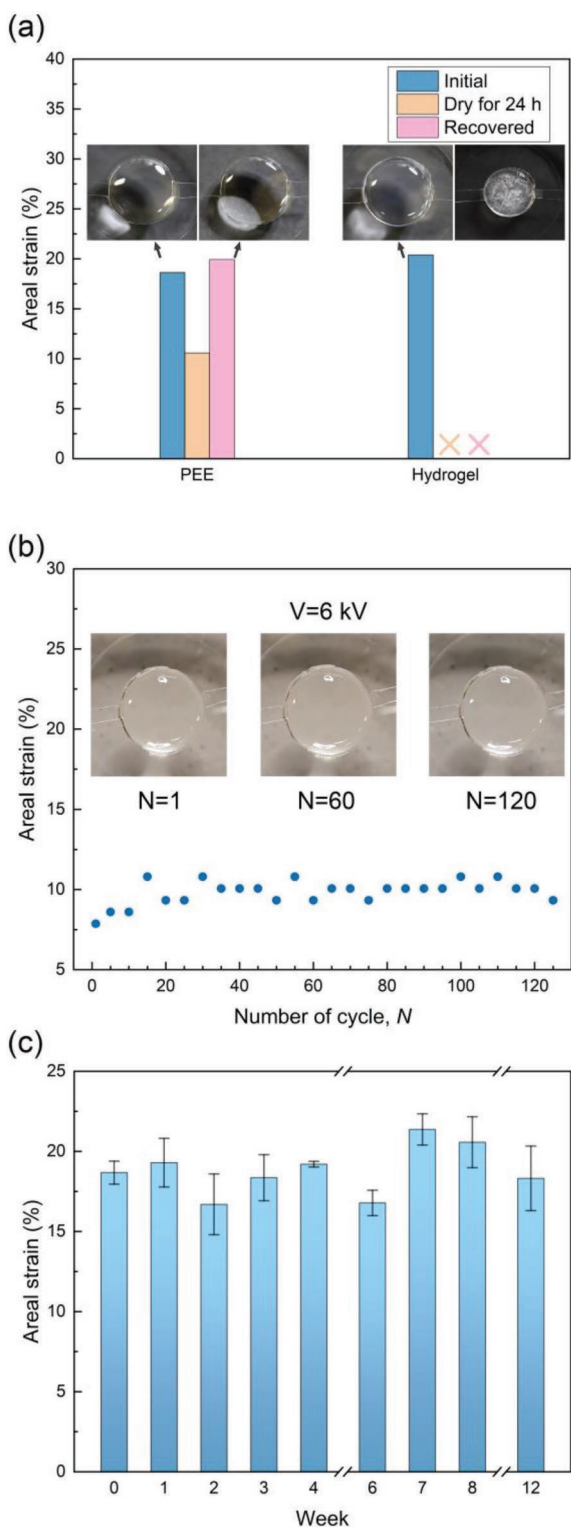


Figure 4. Durability of the tunable lens. a) The areal strain of tunable lens with PEE and ionic polyacrylamide hydrogel as the electrodes under different conditions as indicated. The insets show the corresponding morphologies. The cross symbols imply that the lens fails and no areal strain is available. b) Areal strain varies with the number of cycles under cyclic voltage of magnitude of 6 kV. c) Shelf-life test (sample size $n = 3$).

is on the order of 1 kV. In the tunable lens, the EDL capacitor and the dielectric elastomer capacitor are in series (Figure S9, Supporting Information). Charge balance dictates that $c_{EDL} A_{EDL} V_{EDL} = c_{DE} A_{DE} V_{DE}$, where c , A , and V denote the capacitance per unit area, the area, and the voltage, respectively. Typically, c_{EDL} is on the order of 10^{-2} F m^{-2} . In our experiments, c_{DE} is on the order of 10^{-7} F m^{-2} for a 100- μm -thick VHB, A_{EDL} is on the order of 10^{-5} m^2 , and A_{DE} is on the order of 10^{-4} m^2 , giving $V_{EDL}/V_{DE} = 10^{-4}$. As such, V_{EDL} is below 1 V, so long as the applied voltage is below 10 kV. The charge balance condition implies that the electrochemical breakdown of EDL is more unlikely to occur for a larger A_{DE} , which corresponds to a larger numerical aperture. In addition, we have only used one particular molar ratio of monomer over initiator, i.e., 500:1, and obtained PAPTAC of appropriate mechanical properties. However, the stoichiometric ratio might play a key role in the mechanical properties, which is also the case for PAPTAC (Figure S10, Supporting Information). One can tune the ratio or even add covalent cross-linkers for further optimizations when needed. Last but not least, polyelectrolyte elastomers are hygroscopic in general due to the abundant positive and negative ions. After reaching equilibrium in the ambient environment, polyelectrolyte elastomer typically absorbs a certain amount of water and becomes softer. When exposed to environment of low humidity or high temperature, the absorbed water evaporates and the polyelectrolyte elastomer regains its pristine properties. The change of water content causes the fluctuation of the properties of polyelectrolyte elastomer. To assuage this issue, further research is required to increase the hydrophobicity of the polymer network, for example, using the fluorinated negative ion, bis(trifluoromethanesulfonyl)imide (TFSI).

3. Conclusion

In conclusion, we have reported an all-solid tunable lens driven by a dielectric elastomer actuator based on a soft, stretchable, transparent, and ionically conductive PEE, which functions as not only the refractive component of the tunable lens but also the compliant electrode of the dielectric elastomer actuator. The dual-functional PEE, as well as the proposed mold-free technique, greatly simplifies the structure and the fabrication procedure of the tunable lens. A relative change of focal length exceeding that of the human eye and exceptional stability have been achieved. All-solid tunable lenses of excellent stability offer new opportunities for the designers of tunable optics and are expected to find applications in fields where soft, compact, and reliable vision mechanisms are needed.

4. Experimental Section

Materials: (3-Acrylamidopropyl)trimethylammonium chloride (APTAC, CAS No. 45021-77-0) from Jiuding Chemistry Co. (Shanghai, China), α -ketoglutaric acid (CAS No. 328-50-7) and acrylamide (CAS No. 79-06-1) from Aladdin, and VHB 4910 were purchased from 3M Company. All materials were used as received.

Preparation of Polyelectrolyte Elastomer: APTAC and α -ketoglutaric acid (0.1 mol L^{-1}) were mixed at a mole ratio of 500:1. The solution was injected into a glass mold (100 mm \times 100 mm \times 0.5 mm) and exposed

to ultraviolet light (30 W, 365 nm) for 20 min. Whereas no cross-linkers were added, the cured PEE behaved as a solid that its storage modulus was higher than its loss modulus over the entire range of angular frequency tested in a rheology measurement (Figure S11, Supporting Information).

Fabrication of PEE Tunable Lens: A layer of VHB 4910 was prestretched to $\lambda = 3.3$ by a biaxial stretching machine (Care Measurement & Control, IPBF-300). Two circular acrylic rings (outer diameter 55 mm, inner diameter 45 mm) were aligned and attached firmly to the top and bottom of the prestretched VHB. After being cutoff along the outer periphery, an annular polymer ester film of an inner diameter 15 mm and an outer diameter 45 mm was attached on the VHB. The sample was then subjected to plasma etching (Harrick, plasma cleaner PDC-002) for 3 min. Subsequently, a certain volume of precursor was dripped onto the plasma-etched area and the sample was placed inside a homemade environmental chamber filled with humid nitrogen gas. After 25 min of ultraviolet illumination, the precursor solidified to form a plano-convex lens with a high degree of fidelity of the profile. Finally, copper foils and planar PEE electrodes were attached to complete the fabrication.

Transmittance Measurement: Rectangular PEEs of dimensions of 0.5 mm \times 15 mm \times 30 mm were cut using a laser cutting machine (Epilog, FusionEdge, 90 W). The samples were loaded to the UV-visible spectrophotometer (Metash SH, UV8000) and scanned from 400 to 900 nm at room temperature.

Conductivity Measurement: Rectangular PEEs of dimensions of 0.5 mm \times 15 mm \times 30 mm were prepared. The sample was sealed within a waterproof bag with its two ends connected to a multimeter (Keysight Digit Multimeter, 34465A). The bag was immersed in water, whose temperature was adjusted by adding ice bags or hot water. A thermometer was used to monitor the real-time temperature. Data were recorded after the temperature stabilized.

Mechanical Characterizations: For uniaxial tension, samples were cut into dumbbell shapes of gauge length 18 mm, width 1 mm, and thickness 0.5 mm. The sample was loaded on a universal testing machine (Instron, 5966, 100 N load cell) and pulled at a velocity of 70 mm min⁻¹ at room temperature. For the cyclic tensile test, samples were cut into rectangular shapes of gauge length 40 mm, width 8 mm, and thickness 0.5 mm. The sample was pulled at a velocity of 2 mm s⁻¹ at room temperature. The strain was set as 10% and the number of cycles was 1000 (Figure S12, Supporting Information). For the 90-degree peel, the biaxially prestretched VHB was glued onto an acrylic plate (2 mm \times 100 mm \times 100 mm) and subjected to plasma-etching for 3 min. Afterward, an acrylic frame was attached on VHB, providing a mold of 50 mm in length, 10 mm in width, and 2 mm in thickness. Next, the PEE precursor was filled with the mold, covered with a layer of release film, and cured under ultraviolet light. After the release film and acrylic frame were removed, a piece of nonwoven fabric was glued on the top surface of PEE as a flexible but inextensible backing. Finally, the sample was loaded to the testing machine and peeled at 20 mm min⁻¹. The rheology of PEE was probed using a rheometer (DHR-30, TA) using a flat head (20 mm in diameter). Cylindric specimens with a thickness of 1 mm and a diameter of 20 mm were used. The applied strain was 0.1% and the test was carried out at 25 °C. The glass transition temperature (T_g) was probed using a DSC instrument (DSC-2500, TA). The weight of the sample was 7.3 mg and the scanning temperature ranged from -80 to 80 °C (Figure S13, Supporting Information).

Measurement of Focal Length: A homemade apparatus was used for focal length measurement, which included a slide rail, a parallel light beam, and a screen. The tunable lens was fixed on the slide rail. The light beam was placed on the side of the base of the lens and the screen on the side of the curved surface of the lens. The space of parallel light was set as 11 mm. A black cloth was pasted on the screen to get a clearer light spot. Under a certain voltage, the position of the screen was adjusted until the light spot was the smallest. The distance between the screen and the center of the base of the lens was measured as the focal length at this point. Due to the viscoelasticity of VHB, the focal length was measured a few seconds after a voltage was applied.

Measurement of Response Time: Response time was measured through the frame analysis of a high-speed camera (NAC, Memrecam ACS-3, Macro 100 mm) recording with frames per second of 60, corresponding to a time interval between every two frames of 16.2 milliseconds. The video recording started a few seconds before the voltage was applied and stopped after the areal strain reached the maximum. The areal strain was measured by analyzing the video recorded by a digital camera (Canon, EOS 6D Mark II, Macro 100 mm), which was placed perpendicular to the lens. The time when the areal strain reached 80% of the maximum was taken as the response time of the tunable lens. The basal diameter and the volume of the PEE tunable lens used for response time measurement were 15 mm and 450 μ L, respectively.

Multidepth Object Imaging: A PEE tunable lens with a basal diameter of 15 mm and volume of 450 μ L was vertically installed. A digital camera was fixed at 20 cm from the planar electrode side and three objects, a blue stick, a plastic figure, and a thermo-hygrometer, were fixed at 10, 15, and 45 cm, respectively, from the plano-convex lens side. At voltage-off state, the lens focused on the blue stick. As the voltage increased, the lens focused on the plastic figure at 4 kV and the thermo-hygrometer at 7.4 kV. The high voltage was applied through a high-voltage power supply (Model DW-P503-1ACDF, from Dongwen High-voltage Power Supply Co., Tianjin).

Durability Test: In a test, a PEE tunable lens and an ionic hydrogel tunable lens having the same dimensions were fabricated and their resistances to the desiccated condition were compared. The ionic hydrogel was polyacrylamide hydrogel containing 2 mol L⁻¹ sodium chloride. After initial fabrication, their areal strains were measured at 7 kV. Then, the two lenses were stored in a dry chamber of RH \approx 12% for 24 h and taken out, and their areal strains were measured again. In another test, a PEE tunable lens of 450 μ L in volume and 15 mm in basal diameter was subjected to manually consecutive loading and unloading for 125 cycles at a fixed voltage of 6 kV. The duration time and the time interval before two loadings were 5 s. In addition, the lens was subjected to a sinusoidal voltage of peak 5.7 kV and frequency 1 Hz up to 1000 cycles in the open air. As for the shelf-life test, three tunable lenses were fabricated and their areal strains were continuously monitored at 7 kV weekly. The samples were placed inside petri dishes to avoid contaminations such as dust, stored at room temperature, and tested in the open air. The corresponding ambient humidity and areal strain were recorded for each test (Figure S14, Supporting Information).

Statistical Analysis: Data were collected without preprocessing and presented as the mean \pm SD. In each experiment, the sample size n was at least 3 and had been indicated where applicable. Software used for data analysis included Excel, Origin, Matlab, and ImageJ.

Supporting Information

Supporting Information is available from the Wiley Online Library or from the author.

Acknowledgements

The work at the Southern University of Science and Technology is supported by the National Science Foundation of Guangdong Province (grant no. 2214050008118) and the Science, Technology, and Innovation Commission of Shenzhen Municipality under grant no. (ZDSYS20210623092005017). Y.X. acknowledges the support of the National Natural Science Foundation of China (Nos. 12072225 and 12021002).

Conflict of Interest

The authors declare no conflict of interest.

Data Availability Statement

The data that support the findings of this study are available from the corresponding author upon reasonable request.

Keywords

all-solid state, dielectric elastomer actuators, polyelectrolyte elastomers, stability, tunable lenses

Received: June 10, 2022

Revised: August 30, 2022

Published online:

-
- [1] U. Levy, R. Shamaï, *Microfluid. Nanofluid.* **2008**, *4*, 97.
 [2] K. Mishra, D. Van den Ende, F. Mugele, *Micromachines* **2016**, *7*, 102.
 [3] H. Huang, Y. Zhao, *J. Micromech. Microeng.* **2019**, *29*, 073001.
 [4] Y. Zou, F. S. Chau, G. Zhou, *Opt. Express* **2017**, *25*, 20675.
 [5] F. O. Fahrbach, F. F. Voigt, B. Schmid, F. Helmchen, J. Huisken, *Opt. Express* **2013**, *21*, 21010.
 [6] B. Dai, L. Zhang, C. Zhao, H. Bachman, R. Becker, J. Mai, Z. Jiao, W. Li, L. Zheng, X. Wan, *Nat. Commun.* **2021**, *12*, 6458.
 [7] P. Müller, D. Kopp, A. Llobera, H. Zappe, *Lab Chip* **2014**, *14*, 737.
 [8] M. Jablonowski, *Senses Soc.* **2020**, *15*, 344.
 [9] S. Nam, S. Yun, J. W. Yoon, S. Park, S. K. Park, S. Mun, B. Park, K.-U. Kyung, *Soft Rob.* **2018**, *5*, 777.
 [10] Y. J. Wang, Y. H. Lin, *Opt. Express* **2019**, *27*, 21163.
 [11] L. Chen, M. Ghilardi, J. J. Busfield, F. Carpi, *Front. Robot AI* **2021**, *8*, 678046.
 [12] A. Naumov, M. Y. Loktev, I. Guralnik, G. Vdovin, *Opt. Lett.* **1998**, *23*, 992.
 [13] Y.-H. Lin, Y.-J. Wang, V. Reshetnyak, *Liq. Cryst. Rev.* **2017**, *5*, 111.
 [14] C. P. Chiu, T. J. Chiang, J. K. Chen, F. C. Chang, F. H. Ko, C. W. Chu, S. W. Kuo, S. K. Fan, *J. Adhes. Sci. Technol.* **2012**, *26*, 1773.
 [15] B. Berge, J. Peseux, *Eur. Phys. J. C. Part Fields* **2000**, *3*, 159.
 [16] X. Zeng, H. Jiang, *Appl. Phys. Lett.* **2008**, *93*, 151101.
 [17] T. Krupenkin, S. Yang, P. Mach, *Appl. Phys. Lett.* **2003**, *82*, 316.
 [18] N. Hasan, A. Banerjee, H. Kim, C. H. Mastrangelo, *Opt. Express* **2017**, *25*, 1221.
 [19] T. Peng, C. Dai, J. Lou, Y. Cui, B. Tao, J. Ma, *Opt. Commun.* **2020**, *460*, 125209.
 [20] M. C. Wapler, *Opt. Express* **2020**, *28*, 4973.
 [21] L. Maffli, S. Rosset, M. Ghilardi, F. Carpi, H. Shea, *Adv. Funct. Mater.* **2015**, *25*, 1656.
 [22] S. Shian, R. M. Diebold, D. R. Clarke, *Opt. Express* **2013**, *21*, 8669.
 [23] P. Rasti, H. Hous, H. F. Schlaak, R. Kiefer, G. Anbarjafari, *Appl. Opt.* **2015**, *54*, 9976.
 [24] F. Carpi, G. Frediani, S. Turco, D. De Rossi, *Adv. Funct. Mater.* **2011**, *21*, 4152.
 [25] S. i. Son, D. Pugal, T. Hwang, H. R. Choi, J. C. Koo, Y. Lee, K. Kim, J. D. Nam, *Appl. Opt.* **2012**, *51*, 2987.
 [26] M. Pieroni, C. Lagomarsini, D. De Rossi, F. Carpi, *Bioinspir. Biomim.* **2016**, *11*, 065003.
 [27] S. Liu, Y. Qiu, W. Yu, *Macromol. Mater. Eng.* **2020**, *305*, 2000393.
 [28] B. Chen, W. Sun, J. Lu, J. Yang, Y. Chen, J. Zhou, Z. Suo, *J. Appl. Mech.* **2021**, *88*, 031016.
 [29] H. J. Kim, B. Chen, Z. Suo, R. C. Hayward, *Science* **2020**, *367*, 773.
 [30] D. A. Atchison, G. Smith, G. Smith, *Optics of the human eye*, Butterworth-Heinemann, Oxford **2000**.
 [31] C. Yang, Z. Suo, *Nat. Rev. Mater.* **2018**, *3*, 125.
 [32] C. Keplinger, J. Y. Sun, C. C. Foo, P. Rothemund, G. M. Whitesides, Z. Suo, *Science* **2013**, *341*, 984.
 [33] M. Ghilardi, H. Boys, P. Török, J. J. Busfield, F. Carpi, *Sci. Rep.* **2019**, *9*, 16127.
 [34] X. Li, P. Zhang, Q. Li, H. Wang, C. Yang, *iScience* **2021**, *24*, 102319.
 [35] P. Zhang, Q. Li, Y. Xiao, C. Yang, *ACS Appl. Electron. Mater.* **2021**, *3*, 668.